

The Insignificance of Global Reheating in the Abell 1068 Cluster: Multiwavelength Analysis

B. R. McNamara¹

Dept. of Physics & Astronomy, Ohio University, Athens, OH 45701

mcnamarb@ohio.edu

M. W. Wise

Massachusetts Institute of Technology/Center for Space Research

wise@space.mit.edu

S. S. Murray

Harvard-Smithsonian Center for Astrophysics

ssm@head-cfa.harvard.edu

ABSTRACT

In this paper and in a companion paper, Wise, McNamara, & Murray (2003), hereafter referred to as WMM, we present a detailed, multiwavelength study of the Abell 1068 galaxy cluster, and we use this data to test cooling and energy feedback models of galaxy clusters. Near ultraviolet and infrared images of the cluster show that the cD galaxy is experiencing star formation at a rate of $\sim 20 - 70 M_{\odot} \text{ yr}^{-1}$ over the past $\lesssim 100$ Myr. The dusty starburst is concentrated toward the nucleus of the cD galaxy and in filamentary structures projecting 60 kpc into its halo. The *Chandra* X-ray image presented in WMM reveals a steep temperature gradient that drops from roughly 4.8 keV beyond 120 kpc to roughly 2.3 keV in the inner 10 kpc of the galaxy where the starburst peaks. Over 95% of the ultraviolet and H α photons associated with the starburst are emerging from regions cloaked in keV gas with very short cooling times (~ 100 Myr), as would be expected from star formation fueled by cooling condensations in the intracluster medium. However, the *Chandra* spectrum is consistent with

¹Visiting Astronomer, Kitt Peak National Observatory. NOAO is operated by AURA, Inc. under contract to the National Science Foundation.

but does not require cooling at a rate of $114 - 145 M_{\odot} \text{ yr}^{-1}$, factors of several below the rates found with the *ROSAT* observatory. The local cooling rate in the vicinity of the central starburst is $\lesssim 40 M_{\odot} \text{ yr}^{-1}$, which is consistent with the star formation rate determined with *U*-band and infrared data. We consider energy feedback into the intracluster medium by the radio source, heat conduction, and supernova explosions associated with the starburst. We find that energy feedback from both the radio source and thermal conduction are inconsequential in Abell 1068. Although supernova explosions associated with the starburst may be able to retard cooling in the inner 10 kpc or so of the cluster by $\sim 18\%$ or so, they are incapable of maintaining the cooling gas at keV temperatures. Finally, we present circumstantial evidence for the contrary view that at least some and perhaps all of the star formation may have been fueled by an interaction between the cD and one or more companion galaxies.

Subject headings: galaxies: clusters: general—clusters: cooling flows

1. Introduction

Galaxy clusters frequently possess central cusps of bright X-ray emission from relatively high density, low temperature gas. The radiative cooling time of this gas approaches several hundred million years in the centers of some clusters, which is much shorter than their ages. Unless the thermal energy losses are replenished by a robust heating agent, the gas will cool to low temperatures and sink to the center of the cluster. The natural, long-term repositories for the cooling gas are atomic and molecular clouds and stars. Over the past 20 years, a large body of observational evidence has emerged in support of the existence of such a repository, although at substantially lower levels than expected. The centrally dominant galaxies (CDGs) that lie at the centers of so-called “cooling flows” often harbor cool interstellar media traced by nebular line emission (Heckman et al. 1989, Voit & Donahue 1997), neutral hydrogen (O’Dea, Baum, & Gallimore 1994, Taylor 1996), molecular gas (Edge 2001, Edge et al. 2002, Jaffe & Bremer 1997, Jaffe, Bremer, & Van der Werf 2001, Donahue et al. 2000, Falcke et al. 1998), and star formation (Crawford et al. 1999, Cardiel, Gorgas, & Aragon-Salamanca 1998, McNamara & O’Connell 1989). In addition, a strong correlation exists between the occurrence and strength of star formation in CDGs and the X-ray cooling rates measured with the *Einstein* and *Rosat* observatories (see McNamara 1997, 2002 for reviews). The star formation rates are, however, typically only several to several tens of solar masses per year compared to cooling rates of several hundred solar masses per year. Furthermore, the molecular gas reservoirs that often exceed $\sim 10^{10} M_{\odot}$ in some clusters

(Edge 2001) would in most cases fill to capacity in only several tens of Myr, which is too short a timescale to account for the cooling mass in a long-lived cooling flow. Our inability to account for this apparent mass continuity violation is the crux of the so-called “cooling flow” problem.

Observations of galaxy clusters obtained with the *Chandra* and XMM-Newton observatories have dramatically changed our view of cooling flows. High resolution images obtained with *Chandra* have revealed remarkably complex gaseous structures in the vicinity of the central galaxies (McNamara et al. 2000, 2001, Fabian et al. 2000, and many others). In addition, both the moderate to high resolution spectra obtained with *Chandra*’s ACIS camera and the XMM-Newton’s Reflection Grating Spectrometer do not show the signatures of steady cooling below 2 keV throughout the central regions of clusters (McNamara et al. 2000; Molendi & Pizzolato 2000; David et al. 2001, Fabian et al. 2001, Peterson et al. 2001, Böhringer et al. 2002). Apart perhaps from the very inner regions surrounding the complex X-ray structures, the gas can be adequately modeled as a single temperature plasma. Thus, standard inhomogeneous cooling flow models with gas cooling to low temperatures throughout the central ~ 100 kpc of clusters at a steady rate are apparently incorrect. Nevertheless, the cooling upper limits from *Chandra* and XMM-Newton do not rule-out cooling in the inner regions of clusters at rates ranging between a few and a few hundred solar masses per year (Peterson et al. 2003). These limits are often intriguingly close to the observed levels of star formation in the central cD galaxies. Furthermore, the sites of star formation occur in the vicinity of complex X-ray structures where the cooling time of the gas is less than 3×10^8 years (McNamara et al. 2000, Blanton et al. 2002, McNamara 2002). The local cooling rates surrounding the star formation regions are within factors of several of the star formation rates, as would be expected were star formation fueled by cooling.

The outstanding issue now is whether one or more heating agents capable of preventing wholesale cooling over cosmological timescales can be identified. One such heating agent is the radio source. Most cooling flows contain an audible radio source in their central galaxies (Burns 1990), and they frequently appear to be interacting with the ambient keV gas. For example, large cavities or bubbles have been found in the X-ray emission of many clusters that were evidently created by strong interactions between the central radio sources and the surrounding gas (Böhringer et al. 1993, Carilli et al. 1994, McNamara et al. 2000, Fabian et al. 2000). The energy liberated in *PV* work and by bulk lifting may be sufficient to retard or quench cooling in some objects, although the details of these processes are not understood (Heinz, Reynolds, & Begelman 1998, Reynolds, Heinz, & Begelman 2002, Basson & Alexander 2002, Nulsen et al. 2002, David et al. 2001, Fabian et al. 2002, Kaiser & Binney 2003, Brüggén et al. 2002, Brüggén & Kaiser 2002, Brüggén 2003, Soker et al. 2001, Brighenti & Mathews 2002, Churazov et al. 2001, Churazov et al. 2002, Quilis

et al. 2001, De Young 2003). An additional source of heat may be thermal conduction from the hot outer layers of clusters (Rosner & Tucker 1989, Fabian, Voigt, & Morris 2002, Narayan & Medvedev 2001, Voigt et al. 2002, Soker, Blanton, & Sarazin 2003, Zakamska & Narayan 2003). Acting in concert, a cycle of radio-induced outflow and heat inflow via thermal conduction (Ruszkowski & Begelman 2002) may regulate cooling at the levels of cold gas and star formation observed in CDGs (McNamara et al. 2000, Edge 2001, Edge et al. 2002). *Chandra*’s sharp images now permit the cooling rates to be measured on the same spatial scales as star formation, providing a direct test of cooling and heating models. Applying this test and exploring the consequences of feedback in the Abell 1068 CDG is the purpose of this paper.

We present deep U , R , and $H\alpha$ images of the central region of the $z = 0.1386$ cluster Abell 1068, and we compare them to new *Chandra* imaging discussed in detail in WMM. Abell 1068 was selected among several of the most distant clusters with X-ray evidence for strong cooling flows from the *ROSAT* Brightest Cluster Survey (Allen et al. 1992). The observations were intended to study the star formation strength and morphology of distant CDGs using the stellar population-sensitive U -band and the $H\alpha$ feature. Throughout this paper, we assume $H_0 = 70 \text{ km s}^{-1} \text{ Mpc}^{-1}$, $\Omega_M = 0.3$, $\Omega_\Lambda = 0.7$, $z = 0.1386$, an angular diameter distance of 505 Mpc, and that $1 \text{ arcsec} = 2.45 \text{ kpc}$.

2. Optical Observations

The optical observations were obtained with the Kitt Peak National Observatory 4m telescope’s T2KB CCD camera at prime focus on 1 February, 1995. This configuration delivered a plate scale of 0.47 arcsec/pix. Images were taken through the standard U plus liquid Copper Sulfate red-leak blocking filter, Gunn R , and two intermediate bandwidth filters centered on the redshifted $H\alpha + [\text{N II}]$ features and their adjacent continuum. Total exposure times were 3600 seconds, 800 seconds, 1400 seconds, and 1200 seconds, respectively. The target images were taken in “short scan” mode, which shifts charge in the CCD during an exposure in order to improve the flat field quality of the images. The target images were then individually flat-fielded using twilight sky images, the bias level was subtracted from each image, and the images were combined into the science images used in our analysis.

3. Data Analysis

3.1. Structure of the Central Galaxy

The central 1.2 arcmin (176×176 kpc) of the cluster is shown in the U and R_g bands in Fig. 1. The light in the center of the cluster is dominated by the CDG and two dozen or so fainter galaxies. Both the U -band and R -band images show a wisp of light projected between the CDG’s nucleus and a bright galaxy 15 arcsec to the south-west. A fainter, distorted galaxy is projected 33 arcsec to the north-west of the CDG’s nucleus. In addition, there are several faint knots of light along a line between this galaxy and the CDG. These features, in addition to the CDG’s blue nucleus, will be discussed here in detail.

In Fig. 2 we present the surface brightness profiles of the CDG in U and R_g . The profiles were constructed using elliptical annulae. The annulae have ellipticities of $\simeq 0.4$ and position angles of $\simeq 130^\circ$ matching those of the R -band isophotes at radii between $\sim 10 - 15$ arcsec. The surrounding galaxies were masked from the images in order to isolate the CDG light prior to the analysis. The surface brightness profile in each band was flux calibrated using Landolt standards. The calibrated magnitudes were then transformed from the laboratory frame to the rest frame using K corrections from Coleman, Wu, & Weedman (1980). The K corrections in U and R_g are 0.51 mag and 0.13 mag respectively. The Galactic foreground extinction toward Abell 1068 is very small, thus no correction for foreground extinction was applied. The U and R_g profiles include statistical error bars (imperceptible in all but the outer U -band points), and systematic error confidence intervals (dashed lines) on the U -band profile. The method for determining the confidence intervals is discussed in McNamara & O’Connell (1992).

The R_g profile follows the $R^{1/4}$ law between 1.5 arcsec and 33 arcsec (3.7 – 81 kpc) and over 5 magnitudes of surface brightness. The surface brightness profile rises abruptly a half magnitude above the $R^{1/4}$ profile (straight line in Fig. 2) at a radius of 33 arcsec (81 kpc) and surface brightness of 25 mag per square arcsecond and remains there to the limiting radius of our photometry. This departure above the $R^{1/4}$ profile is the signature of an envelope, which is the defining characteristic of a cD galaxy (Schombert 1986). Therefore, we will use the terms cD and CDG interchangeably when describing Abell 1068’s central galaxy. The U -band profile likewise follows an $R^{1/4}$ profile between 4 arcsec and 33 arcsec (10 kpc and 81 kpc). Beyond this radius the surface brightness profile likewise rises above the $R^{1/4}$ law. Apart from the blue core, these properties are typical of central cluster galaxies within a redshift $z \lesssim 0.1$ (Porter et al. 1991).

Within a radius of 4 arcsec (10 kpc) the U -band profile brightens by nearly a magnitude compared to the $R^{1/4}$ profile. In Fig. 3 we show the $(U - R)_{K,0}$ color profile derived from the

surface brightness profiles in Fig. 1. To establish a point of reference, the normal rest-frame colors for a cD galaxy generally lie within the range of 2.3 – 2.6. The nuclear colors tend toward the red end of this range (Peletier et al. 1990). The cD’s $U - R$ color becomes approximately 0.9 magnitudes bluer than normal in the central 4 arcsec. Beyond 4 arcsec the color profile remains roughly constant at a value of $(U - R)_{K,0} \sim 2.3$ well into the halo of the galaxy.

3.2. Blue Morphology of the Central Galaxy

In addition to the the blue nucleus, there are several anomalously blue structures projected onto the halo of the cD galaxy. In Fig. 3 we present a U -band image of the central galaxy after subtracting a smooth stellar model. The residual image clearly shows the two dozen or so galaxies and the wispy features seen in Fig. 1. We placed letters on the map to identify features of interest. The blue nucleus, A , is at the center of the figure indicated with a “+”. Eight arcsec to the north-west at B lies an arc-like feature with a faint light bridge to the nucleus. Extending from B , a wisp of light, C , curves 22 arcseconds to the south-west toward the nucleus of a bright galaxy, D . A fainter galaxy, E , is seen 36 arcsec to the north-west of the nucleus. What appear to be either small galaxies or debris near F are seen between A and galaxy E .

Fig. 3 includes a color map of this region on the same spatial scale superposed onto the R_g isophotal contours. Relatively normal colors are shown in white and the unusually blue regions are shown in blue. As expected, the region within a 4 arcsec radius of the nucleus is blue, as are features B , C , and F . Note the normal nuclear colors of galaxies D and E . Colors, magnitudes, and average surface brightnesses of these regions are given in Table 1. The bluest region outside the nucleus is the bright arc C . Adopting $(U - R)_{K,0} \sim 2.3$ as the typical color of giant elliptical star light, region C is 0.2–0.6 magnitudes bluer than normal. Likewise, features B and F are ~ 0.2 magnitudes and $\sim 0.4 - 0.5$ magnitudes bluer than normal, respectively.

The integrated magnitudes of galaxies D and E (Table 1) are $R_g = 16.94$ and $R_g = 18.53$, respectively, corresponding to absolute magnitudes $M(R_g) = -22.1$ and $M(R_g) = -20.6$, or equivalently, $1.3L^*$ and $0.3L^*$, respectively. They are clearly massive galaxies whose colors are consistent with those of giant ellipticals or perhaps spiral bulges. We see no star formation within these galaxies, and they appear to be interacting with the cD. If they are triggering star formation in the process, galaxies D and E are more likely to be disrupted spiral bulges rather than giant ellipticals (cf., §7).

The arc-like features B and C are noteworthy in that we cannot exclude the possibility that one or both are gravitational arcs, rather than local star formation. The more compelling gravitational arc would be B , as it appears to be centered on the cD galaxy, which is presumably the local center of mass. However, inspection of Figures 3 and 4 shows that this feature is associated with a “hook” of $H\alpha$ emission (discussed in detail in the next section), which would be a surprising coincidence were the feature indeed a gravitational arc. The more likely interpretation of this unusual feature is star formation triggered by an interaction with the radio source shown in Figure 4. Feature C represents a poorer case for a gravitational arc because its radius of curvature is much larger than its radial distance from the cD, and it is not centered on the cD. On the other hand, strong $H\alpha$ emission is absent toward this feature, and toward the apparent debris trail at E and F , which weakens to some degree the case for star formation in these regions. However, the absence of strong $H\alpha$ emission toward arc C and the debris trail is probably a consequence of their low optical luminosities and correspondingly low local star formation rates. In any event, the true interpretation of the arc-like features would have only a minor impact on the conclusions of this paper.

3.3. Nebular Emission

In Fig. 4 we present an $H\alpha + [NII]$ map of the cD. A bright, extended emission-line nebula is centered on the cD and is somewhat more extended than the blue nucleus. The nebula is irregular in shape with a tongue of emission extending to the north-west terminating in a knot of emission at the blue, arc-like feature B . The $H\alpha$ luminosity is $\gtrsim 10^{42}$ ergs s^{-1} (Allen et al. 1992). The surface brightness profile of the emission nebula is shown as crosses in Fig. 2, scaled arbitrarily to show its spatial extent relative to the U -band excess. It is sharply peaked on the cD’s nucleus but drops below detectability at a radius of 10 arcsec, where the northern tongue of emission terminates. In this respect, Abell 1068 is similar to other cooling flow clusters harboring luminous emission nebulae (eg., Heckman et al. 1989, Crawford et al. 1993).

3.4. The Radio Sources

Both the cD and the bright galaxy D to the south-west are 20 cm *FIRST* survey radio sources (White et al. 1997, Gubanov & Reshetnikov 1999). For reference, the 5 arcsec resolution radio map is superposed on the U -band contours in Fig. 4. Their radio fluxes are 8.71 ± 0.14 mJy and 10.87 ± 0.14 mJy, respectively. The cD’s radio source is marginally resolved and extends along position angle $\simeq 150^\circ$ in the direction of the tongue of $H\alpha$

emission to the north-west. Both the radio source and the tongue of H α emission terminate at the location of the bright blue arc B . A close spatial relationship between the radio source, nebular emission, and knots of star formation is a common pattern in powerful radio galaxies and in cooling flows. Abell 1068 seems to fit this pattern.

3.5. Cold Gas and Dust

The infrared source F10378+4012 lies at the position of the cD. The *IRAS* Faint Source Catalog lists its 60 and 100 micron fluxes as 577 mJy and 958 mJy respectively. Combined, they imply a total infrared flux of 3×10^{-11} erg s $^{-1}$ cm $^{-2}$ (cf., Wise et al. 1993). At Abell 1068’s distance, the corresponding total infrared luminosity is $L_{\text{FIR}}(40 - 500\mu\text{m}) \geq 1.5 \times 10^{45}$ erg s $^{-1}$. Assuming the infrared light is being emitted by dust grains, the dust temperature and mass are 31 K and $2 \times 10^8 M_{\odot}$ respectively. The location and spatial extent of the infrared emission region is unknown, but is probably associated with the starburst. Assuming the dust is distributed in a foreground screen of 10 kpc radius with scattering properties similar to dust in our galaxy, the visual extinction and color excess would be $A_V \sim 4.3$ and $E(B - V) \sim 1.4$ magnitudes, respectively. Extinction with these properties would be readily apparent in our optical images, and the color excess would be much larger than $E(B - V) = 0.39$ found by Crawford et al. (1999) based on the anomalous Balmer decrement in the emission nebula. This inconsistency implies that the dust is either confined to very small scales, or is broadly distributed throughout the cluster.

Greater than $4 \times 10^{10} M_{\odot}$ of molecular gas has been detected at millimeter CO ($2 \rightarrow 1$) and CO($1 \rightarrow 0$) features (Edge 2000), and in the 2μ lines of molecular hydrogen (Edge et al. 2002). The apparently close spatial association of the 2μ emission and H α emission in this and other cooling flows (Donahue et al. 2000) suggests that the molecular material, and probably the dust are closely associated with the starburst. The gas to dust ratio implied by the *IRAS* and CO data must be $\gtrsim 200$, which is in line with other clusters (Edge 2001). Edge pointed out that Abell 1068’s high infrared luminosity and its abundance of molecular gas are properties in common with those of the luminous infrared galaxies (Sanders & Mirabel 1996).

3.6. Star Formation in the Central Blue Structure

Anomalously blue colors are observed in many cooling flow CDGs. Although most are associated with star formation, blue color excesses can be caused by metal poor stellar pop-

ulations or emission from active nuclei. The normal central colors of CDGs lie in the range $(U - R)_{K,0} \sim 2.3 - 2.6$ (Peletier et al. 1990). A normal giant elliptical galaxy becomes bluer with increasing radius by roughly two tenths of a magnitude per decade in radius (Peletier et al. 1990). By comparison, normal central cluster galaxies have somewhat shallower gradients, and sometimes may redden with increasing radius (Mackie 1992, McNamara & O’Connell 1992). A gradual blueing with increasing radius is thought to originate in populations of decreasing average stellar metallicity, decreasing age, or a decreasing level of dust absorption. The general trend for ellipticals to possess red, metal enhanced or dusty cores is inconsistent with the blue core in Abell 1068. Therefore, it cannot be explained straightforwardly as a metallicity effect within the usual context of giant ellipticals.

Emission from an active nucleus is a possible origin for the central blue colors, but it would have difficulty explaining Abell 1068’s overall properties. The nuclear blue emission is distributed almost symmetrically about the nucleus, and there is no evidence for anisotropies associated with beamed nuclear radiation. Assuming this light is being scattered isotropically from a central source, we would expect to see a bright central peak and faint halo structure with a large contrast ratio due to the inefficient scattering of photons by electrons and dust. This is not seen, nor is a point source seen in the *Chandra* X-ray image. Finally, we and others (Allen et al. 1992, Allen 1996, and Crawford et al. 1999) have shown that the blue core is associated with nebular emission whose line ratios are a closer match to H II regions than AGN. Taken together, Abell 1068’s properties are consistent with ongoing massive star formation; we will proceed with this assumption.

4. Star Formation History of the cD Galaxy

4.1. The Nuclear Starburst

Our primary objective is to explore the well known relationship between star formation and the centrally-peaked, cluster X-ray emission. *Chandra*’s high spatial resolution provides for a direct comparison between the star formation regions and X-ray emission on the same arcsec spatial scales. This unique capability provides a crucial test of the cooling paradigm, which we apply in this section of the paper.

In order to estimate the star formation rate, or more precisely, the luminosity mass of the young stellar population, we measured the fraction of the *U*-band light emerging from the blue population in the inner 4 arcsec radius ($\simeq 10$ kpc) by modeling the *U*-band light of the host galaxy using an $R^{1/4}$ -law surface brightness profile with a softened core. The fraction of light, f_{AP} , contributed by the blue “accretion population” was found by subtracting the

model U -band image of host galaxy from the real image, leaving the accretion population in residual. This analysis shows that the accretion population contributes up to 75% of the U -band light in the inner arcsec, and averages 12% over the inner 4 arcsec radius region. We determined the mass of the accretion population as $M_{\text{AP}} = M/L(U)_{\text{AP}} f_{\text{AP}} L(U)$, where $M/L(U)_{\text{AP}}$ is the U -band mass-to-light ratio of the accretion population, and $L(U)$ is the total U -band luminosity of the central blue region. The stellar population histories are based on the Bruzual & Charlot (1993) population models with the Salpeter initial mass function and Solar abundances. We found the U -band luminosity of the accretion population alone to be $L(U)_{\text{AP}} \equiv f_{\text{AP}} L(U) = 2 \times 10^{10} L_{\odot}$, before correcting for extinction.

Measuring the intrinsic color of the accretion population is the most difficult aspect of this analysis. The color constrains the population’s age and history, which in turn is used to estimate its mass-to-light ratio by comparison to stellar population models. The accuracy of the measurement is limited by our ability to separate the light of the accretion population from the surrounding glare of the background cD galaxy. While the U -band signal from the accretion population is relatively strong and therefore somewhat easier to model, the fraction of the total light contributed by the accretion population in the R -band is only $\sim 5\%$. Such a small contribution to the total light implies that a small error in the galaxy model can lead to a substantial misestimation of the R -band flux, and a correspondingly large error in the accretion population’s color. Adding to these difficulties, the light from the accretion population is heavily concentrated toward the nucleus where its light fraction varies dramatically with radius. Furthermore, the true central surface brightness profile of the background population at U is poorly determined. With these caveats in mind, we find a probable range for the central accretion population color of $(U - R)_{\text{AP}} \sim -0.1$ to -0.3 .

This color range is broadly consistent with two star formation histories: continuous star formation with a range of ages, and a simple, instantaneous burst (cf., Table 2). For the blue end of the color range, the instantaneous burst and continuous star formation histories are indistinguishable, having ages of $\sim 6 - 10$ Myr and similar mass-to-light ratios. The red end of the color range is consistent with ongoing star formation for ~ 100 Myr, or an aging burst that occurred roughly 40 Myr ago. The continuous star formation history brackets a 10 Myr to 100 Myr time span at rates between $40 M_{\odot} \text{ yr}^{-1}$ and $16 M_{\odot} \text{ yr}^{-1}$, respectively. The corresponding accretion population masses would be $4 \times 10^8 M_{\odot}$ and $1.6 \times 10^9 M_{\odot}$, respectively. The colors are equally consistent with a fading, instantaneous burst that occurred between 6 Myr and 40 Myr ago, with corresponding accretion population masses of $4 \times 10^8 M_{\odot}$ and $10^9 M_{\odot}$, respectively. The uncertainty in our color measurement does not permit a precise reconstruction of the star formation history. However, the additional constraints discussed below suggest the starburst has consumed a small fraction of the available molecular fuel, and may be in the early stages of a more extended episode of star formation.

4.2. Off Nuclear Star Formation

An inspection of Fig. 3 shows a series of blue regions lying at angular distances of between a few and several tens of arcsec from the nuclear starburst. These regions are described in §3.2 and their apparent colors and magnitudes are given in Table 1. The large arc at location *C* is two tenths of a magnitude bluer than the nucleus, while the smaller arc at *B* is two tenths of a magnitude redder than the nucleus. The colors include light from the background cD galaxy and do not represent the intrinsic colors of the blue population themselves. Using procedures similar to those described above, the intrinsic colors of the off nuclear blue features range between $U - R_{K,0} \sim -0.2$ to $U - R_{K,0} \sim 0.1$. This color range brackets those of the nucleus and extends redward. The total *U*-band luminosity of the off-nuclear regions is $5 \times 10^9 L_{\odot}$, only one quarter that of the nuclear *U*-band luminosity (Table 2).

In order to interpret the colors and luminosities in terms of an average star formation history, we combined the off-nuclear blue light from regions *B*, *C*, & *F*, and summarized their properties in Table 2. The color range of the off nuclear population is consistent with a short duration burst that occurred between 7 and 50 Myr ago, with a corresponding luminosity mass between $\sim 0.9 - 3 \times 10^8 M_{\odot}$, and with constant star formation at a rate of between $3 - 5 M_{\odot} \text{ yr}^{-1}$ that has been ongoing for 100 – 500 Myr. The physical appearance of the population and its possible association with an interaction between the cD and two of its neighbors favors the burst history.

4.3. Far Infrared Star Formation Rate

The far infrared luminosity in the direction of the cluster was found to be $L_{\text{FIR}}(40 - 500\mu\text{m}) \geq 1.5 \times 10^{45} \text{ erg s}^{-1}$ in §3.5. Assuming all of the infrared flux is processed ultraviolet light from the starburst, the star formation rate based on the global Schmidt law for spiral and starburst galaxies (Kennicutt 1998) is $68 M_{\odot} \text{ yr}^{-1}$, with a formal uncertainty of $\sim 50\%$. This figure is only 1.5–3.5 times larger than our estimates in Table 2, and is well within the uncertainties of the measurements. Taking the optical and infrared star formation rates at face value, the star formation region is largely obscured, and most of its radiation is emerging in the infrared.

5. Star Formation Fueled by Cooling

If star formation is being fueled by cooling condensations in the X-ray gas, we expect to find the coolest gas with the shortest cooling time in close proximity to the regions of star formation. In order to test this condition, we compare the blue regions with the temperature map in Fig. 5, and to the isobaric cooling time profile, Fig. 12b in WMM. The temperature map, shown with the same centering and spatial scale as the optical images in Figs. 1, 3, & 4, shows a great deal of structure. Three distinct concentrations of cool gas are evident. The coolest concentration shown in dark blue is centered on the cD. The second extends to the south-east of the cD, and a third extends to the west.

The coolest gas in the cluster at $\simeq 2.5$ keV is projected on the cD's inner $\simeq 6$ arcsec coincident with the nebular emission and the region from which $\sim 75\%$ of the U -band light from the young stellar population is emerging. Fig. 12b in WMM shows that the isobaric cooling time is $\sim 10^8$ yr in the inner 10 kpc, and then rises to $\sim 10^9$ yr at a radius of 100 kpc, reaching a value of $\sim 10^{10}$ yr at a radius of ~ 200 kpc. The gas in the central starburst region has the shortest isobaric cooling time in the cluster $t_c \simeq 9 \times 10^7$ yr. This trend is seen in other objects such as the Hydra A and Abell 1795 clusters (McNamara et al. 2000, Fabian et al. 2000).

The situation with the off-nuclear star formation is less clear. Regions B and C , which contain $\sim 23\%$ of the blue light, are located within the tongue of cool gas extending to the west of the cD. The gas surrounding this region has a short cooling time of $t_c \sim 5 \times 10^8$ yr. On the other hand, the blue knots of star formation at F are in a higher temperature region with a cooling time exceeding $\sim 10^9$ yr. The connection of this material to cooling is less compelling, although it accounts for only 2% of the excess U -band luminosity. This material may instead be associated with debris that has been stripped from the nearby galaxy at E . It is worth noting that no obvious star formation is associated with the tongue of cool gas that extends 20 – 30 arcsec south-east of the cD, although we cannot exclude the possibility of a faint, diffuse population of young stars there.

5.1. Comparison Between Cooling Rates and Star Formation Rates

In WMM, we reported several emission models capable of reproducing the X-ray spectra of the gas in the central 100 kpc of the cluster. The maximum total cooling rate of roughly $1000 M_\odot \text{ yr}^{-1}$ is comparable to those found in earlier *ROSAT* analyses (eg., Allen 2000). This model is not well fit to the data. Furthermore, the cooling stops at 2 keV, with very little cooling flux at lower energies. This behavior, which is now commonly seen clusters,

indicates that little gas is cooling to low temperatures, or much of the gas is cooling to low temperatures with a low radiative efficiency (Fabian et al. 2000).

Spectral models exist that fit the X-ray spectra reasonably well that require gas to cool to very low temperatures, albeit at much smaller rates (WMM). These “full cooling” models constrain the maximum level of cooling below X-ray temperatures to be $114 - 145 M_{\odot} \text{ yr}^{-1}$ (depending on the assumed foreground hydrogen column density) to a radius of ~ 200 kpc, well beyond the star formation radius. The deprojected full cooling rate in the central 5 arcsec of the cD galaxy, where most of the star formation is occurring, is $\dot{m} = 45 \pm 20 M_{\odot} \text{ yr}^{-1}$. This local cooling rate agrees with the the measured range of constant star formation $\dot{s} \sim 20 - 68 M_{\odot} \text{ yr}^{-1}$. The high value is the far infrared star formation rate discussed earlier. The probable mass of the accretion population ranges between $4 \times 10^8 M_{\odot}$ and $2 \times 10^9 M_{\odot}$, a small fraction of the molecular gas mass, $4 \times 10^{10} M_{\odot}$ (Edge 2000). Considering the star formation analysis above, this would suggest that star formation will continue over an extended period of time, and not in a short duration burst. If the molecular gas is fueling the star formation at the level of $15 - 70 M_{\odot} \text{ yr}^{-1}$, star formation will be quenched in roughly one Gyr, assuming no new cold material is accreted. It is therefore likely that star formation is in its early stages.

6. Feedback & Reduced Cooling in the Clusters’s Core

It became apparent from the earliest cluster observations with *Chandra* (McNamara et al. 2000; Fabian et al. 2000) and *XMM-Newton* (Molendi & Pizzolato 2001; Peterson et al. 2001) that the cooling rates reported from the previous generation of X-ray observatories were either vastly overestimated, or that cooling must be occurring with a very low radiative efficiency (Fabian et al. 2000, Böhringer et al. 2002). The former hypothesis implies the gas is being maintained at X-ray temperatures by a heating agent. Possibilities include the radio sources in cD galaxies (Rosner & Tucker 1989), heat conduction from the hot outer layers of clusters (Narayan & Medvedev 2001), and supernova explosions associated with star formation in the cooling gas (Silk et al. 1986). The interest in radio sources has been revived by *Chandra*’s discovery of X-ray cavities or bubbles associated with radio sources in clusters (see McNamara 2002 for a review). Although some models appeal to direct heating by the radio source (eg., Tucker & David 1997, Soker et al. 2000, Binney & Kaiser 2002), the cool rims of the cavities (McNamara et al. 2000, Fabian et al. 2000, Nulsen et al. 2002) are inconsistent with this model (but see Brighenti & Mathews 2002). Some have suggested that the bubbles prevent cooling by lifting cool, low entropy gas from the central regions of clusters outward, where it can expand and mix with hotter gas (David et. al. 2001, Nulsen et

al. 2002, Brüggén & Kaiser 2002, Churazov et al. 2002). On the other hand, the convective lifting of material to large radii should erase the observed metallicity gradients in the gas (Nulsen et al. 2002), unless the metals are rapidly replenished.

Recent theoretical studies have focussed on the most powerful radio sources such as Hydra A (Nulsen et al. 2002, Binney & Kaiser 2002). While $\sim 70\%$ of cooling flow cluster central galaxies are radio audible (Burns 1990), their typical luminosities are often one or two orders of magnitude below the most powerful cluster sources such as Hydra A. It has not been shown that radio sources are generally capable of significantly reducing or quenching cooling without help from additional heating agents (McNamara 2002). In an interesting hybrid model, the radio source heats from the center of the cluster while thermal conduction from the cluster’s hot halo heats the core from the outside (Ruszkowski & Begelman 2002). Their hydrodynamic model appears to reproduce qualitatively the observed radial temperature, density, and entropy, distributions of clusters, while producing intermittent cooling at dramatically reduced levels. In this section, we test these models against the Abell 1068 data by comparing the energy available from supernova explosions, the radio source, and heat conduction to the X-ray luminosity of the cooling gas.

The power required to reheat the intracluster medium and maintain the gas at keV temperatures must exceed the cooling luminosity of the gas. The luminosity of the gas cooling from the ambient temperature of ~ 4.5 keV through the low energy cutoff in the X-ray band of ~ 0.1 keV is given by:

$$L_{\text{cool}} \simeq 1.1 \times 10^{42} \left[\frac{\dot{M}}{1 \text{ M}_{\odot} \text{ yr}^{-1}} \right] \left[\frac{\Delta T}{4.4 \text{ keV}} \right] \text{ erg sec}^{-1}.$$

For cooling at the level of $114\text{--}145 \text{ M}_{\odot} \text{ yr}^{-1}$ (WMM), we find $L_{\text{cool}} \simeq 1.3\text{--}1.6 \times 10^{44} \text{ ergs s}^{-1}$. In order to quench cooling, the total energy of all heating mechanisms must be exceed this value, since the coupling between the heating mechanisms and the gas will not be perfectly efficient. Furthermore, in order to quench cooling over long timescales, the heating must also persist over long timescales.

6.1. Heating by Supernova Explosions

Assuming that star formation has proceeded at a constant rate of between $21 \text{ M}_{\odot} \text{ yr}^{-1}$ (the sum of the nuclear and off-nuclear constant star formation given in Table 2) and $68 \text{ M}_{\odot} \text{ yr}^{-1}$ (the infrared rate), the total mass of the young population would be $2.1\text{--}6.7 \times 10^9 \text{ M}_{\odot}$. Further assuming a Type II supernova explosion rate of one per 100 M_{\odot} of

star formation, we expect that $2.1 - 6.7 \times 10^7$ explosions have occurred in the starburst region in the past 100 Myr. Taking the total kinetic energy deposited into the intracluster medium to be $\sim 10^{51}$ erg per explosion, then $\sim 2.1 - 6.7 \times 10^{58}$ erg has been deposited by Type II supernovae over the past 100 Myr. Energy input at this level would correspond to a feedback luminosity of $\sim 0.7 - 2.1 \times 10^{43}$ erg sec $^{-1}$.

Drawing upon the discussion of the Type I supernova rate in WMM, the Type I rate integrated over the coolest region of the cluster is 0.03 yr $^{-1}$. This amounts to a feedback luminosity of $\sim 10^{42}$ erg s $^{-1}$, less than one tenth of the energy supplied by the starburst. The total feedback luminosity from both Type I and Type II supernova explosions then ranges between $\sim 8 \times 10^{42}$ erg s $^{-1}$ and $\sim 2.3 \times 10^{43}$ erg sec $^{-1}$. This provide up to $\sim 18\%$ of the cooling luminosity. Therefore, supernova explosions can reduce the level of cooling. However, unless the supernova or star formation rates are in error by at least five times, they would be unable to stop cooling entirely.

6.2. Heating by the Radio Source & Thermal Conduction

Now we turn to feedback from the radio source. The monochromatic radio luminosity of the cD at 1.4 GHz is 6.26×10^{39} ergs s $^{-1}$, based on the *FIRST* survey image. The radio source is barely resolved in this image (Fig. 4), and cannot be separated into a core and lobe structure, if one exists at all. The spectral slopes of radio sources can vary widely from $\sim \nu^{-0.7}$ for radio cores to $\sim \nu^{-1.5}$ for radio lobes. Therefore, for simplicity we will assume Abell 1068's radio spectrum obeys a power law of form $F_\nu \sim \nu^{-1}$ between $\nu = 0.01 - 3$ GHz (our conclusions are relatively insensitive to the choice of slope). The total radio luminosity would then be $L_{\text{rad}} = 3.57 \times 10^{40}$ ergs s $^{-1}$. To address the concerns of energy deposition into the hot gas, the total mechanical energy, not the total radiation, is relevant. The radiative efficiency of radio jets is probably less than unity, such that the total mechanical energy may be a factors of 10 – 100 times larger than the radio power. This consideration would imply a total mechanical energy of $\sim 3.57 \times 10^{41 \rightarrow 42}$ ergs s $^{-1}$ heats the intracluster medium over the lifetime of the radio source, or up to $\sim 3\%$ of the cooling luminosity.

Bear in mind the crude nature of these calculations. For example, the radiative efficiency of the radio source, which we have assumed to lie between 1 – 10%, is not well understood. In order to balance cooling, the radiative efficiency would have to be lowered to values approaching $\sim 0.02\%$, which seems implausibly low. Were the radiative efficiency indeed this low, the radio source would interact strongly with the hot gas leaving observable signatures, such as the cavities observed in other clusters. The energy expended in *PV* work alone would create cavities 10 – 20 kpc across. No cavities are observed. Furthermore, the correlation

between contours of excess central metallicity and the cD’s stellar isophotes (see WMM), are consistent with a central metallicity gradient buildup over the past ~ 3 Gyr. This gradient suggests that the gas has not been significantly mixed by the lifting action of bubbles, which would act to diminish the metallicity gradient. Therefore, it seems unlikely that the current radio source or others in the recent past would be capable of substantially reducing cooling.

In Wise, McNamara, & Murray (2003), we excluded heat conduction from the outer layers of the cluster as an important source of heat in the inner regions (Narayan & Medvedev 2001, Zakamska & Narayan 2003). Assuming conduction is proceeding at the Spitzer rate, we found the inward heat flux to be well below the cooling flux throughout the cluster.

In summary, heating by the radio source and thermal conduction seems to be inconsequential. The dominant heating agent appears to be supernova explosions in the inner 10 kpc or so associated with the starburst. Supernova heating at a rate of $\sim 2 \times 10^{43}$ ergs s^{-1} should persist for \lesssim Gyr before the starburst has exhausted its fuel, which would be capable of reducing the cooling rate by only 10% – 20%, provided they are efficiently coupled to the hot gas.

7. A Dynamically Induced Starburst?

Although perhaps the less compelling interpretation, the starburst in Abell 1068 could be unrelated to cooling, but was triggered by a tidal or ram pressure interaction. While the optical data are too crude to distinguish between star formation histories of a dynamically-triggered starburst or a cooling flow, other circumstantial evidence can be cited in support the interaction hypothesis. First, the star formation regions extend well into the envelope of the cD galaxy, and galaxies *D* and *E* appear to be associated with the off-nuclear star formation. Galaxy *E* appears disrupted with blue debris extending toward the cD. It could originally have been a gas-rich spiral galaxy that was tidally disrupted and ram-pressure stripped as it traversed the high density cluster core. Secondly, the cD harbors a large reservoir of molecular gas (§3.5). While neutral hydrogen would have been stripped from the galaxy before it arrived at the center of the cluster, high density molecular clouds tend to inhabit the tightly-bound inner regions of galaxies. These clouds are more likely to survive the plunge through the cluster’s halo before being ripped out by the cD and its associated X-ray halo as they arrive in the core. In addition, the Abell 1068 cD is a luminous infrared galaxy, and both are radio sources. This combination of features is commonly seen in dynamically-triggered starbursts (Sanders & Mirabel 1996). While these properties may be circumstantial and unconvincing, they are certainly suggestive.

Finally, inspection of Fig. 1 in WMM shows a filament or trail of X-ray emission extending from the cD toward galaxy *E*. The temperature map also shows a cool, bow-shaped structure to the south-east of the cD is reminiscent of a moving mass of cooler gas, perhaps from a group that has just fallen into the cluster. Filaments or trails of enhanced density and X-ray emission were predicted to occur during ram pressure interactions in clusters by Stevens, Acreman, & Ponman (1999). The enhancements are created by gravitational focusing in a process analogous to Bondi-Hoyle accretion, or by the stripped debris itself. A gravitationally-focussed trail may also be created by the cD as it sloshes about in the center of the cluster. A strikingly similar situation may be seen in Abell 1795, where an X-ray filament ~ 70 kpc in length (Fabian et al. 2002) is associated with a filament of $H\alpha$ emission (Cowie et al. 1983) and star formation (McNamara et al. 1996). In both instances, several disrupted satellite galaxies are associated with the debris. Whatever their origin, star formation associated with the trails contributes only a small fraction of the ultraviolet light from the starbursts. Therefore, the interaction may be contributing to a centrally-condensed, cooling-fueled starburst but is unlikely to be the dominant mechanism, unless the cold material exchanged in the interaction quickly makes its way to the cD’s nucleus. It is also possible that the trails are simply cooling condensations. Distinguishing between these scenarios will require more detailed hydrodynamical simulations along the lines of Stevens, Acreman, & Ponman (1999) and more sensitive ultraviolet and X-ray data.

8. Conclusions & Discussion

In this paper and in the companion paper WMM, we presented a multiwavelength analysis of the Abell 1068 galaxy cluster featuring a new *Chandra* X-ray image of the cluster. We compared the levels of cold molecular gas and star formation to the maximum cooling rates of the intracluster medium allowed by the X-ray data. In addition, we calculated the energy returned to the intracluster medium from the radio source, supernova explosions, and thermal conduction, and we evaluated their ability to reduce or quench cooling. In addition, we searched for correlations between regions of intense star formation and cooling condensations in the keV gas. We used our analysis to test the self-regulated cooling flow paradigm.

The near ultraviolet and infrared colors and luminosities are consistent with either a short-duration burst of star formation that occurred between 6 Myr and 40 Myr ago, or continuous star formation over the past 10 Myr to 100 Myr at a rate of between $16 M_{\odot} \text{ yr}^{-1}$ and $70 M_{\odot} \text{ yr}^{-1}$. The existence of a central reservoir of $\sim 4 \times 10^{10} M_{\odot}$ of molecular gas suggests that Abell 1068 is in the early stages of star formation that will continue for nearly

\sim Gyr.

The *Chandra* data show the sharp drop in central gas temperature that is the characteristic signature of a cooling flow. The temperature drops from $\simeq 4.5$ keV beyond 100 kpc to ~ 2 keV in the central starburst region of the cD. More than 95% of the ultraviolet and H α photons from the starburst are emerging from regions where the cooling time of the hot gas is less than $\sim 5 \times 10^8$ yr. The upper limit on cooling below X-ray temperatures is $\lesssim 115 - 145 M_{\odot} \text{ yr}^{-1}$. This figure is several times smaller than the rate of cooling between the ambient cluster temperature and ~ 2 keV, and the total cooling rates found with the *ROSAT* observatory. In this respect, Abell 1068 is similar to other clusters studied with the *Chandra* and XMM observatories which appear to be cooling rapidly between ambient cluster temperatures and 2 Kev, but show few of the expected signatures of cooling to lower temperatures. The new cooling rates agree with the star formation rates to within factors of 2 – 3, which are within the measurement uncertainties.

Neither the radio source nor heat conduction are capable of substantially reducing the level of cooling in Abell 1068. However, supernova explosions associated with the starburst may be capable of reducing cooling by $\simeq 20\%$. This result is inconsistent with new self-regulated cooling models that are able to maintain most of the cooling gas at keV temperatures through a variety of heating processes. However, this apparent inconsistency may reflect the possibility that we are observing Abell 1068 during a transient period of rapid cooling and intense star formation that will eventually be slaked by a future radio outburst.

Finally, we presented circumstantial evidence that the the starburst was triggered or enhanced by a tidal or ram pressure interaction with two or more neighboring galaxies. The X-ray and optical features in Abell 1068 and other clusters with dense X-ray cores are qualitatively similar to gravitational wakes and cool debris seen in hydrodynamical simulations (Stevens, Acreman, & Ponman 1999). As more sensitive observations in the X-ray and the far ultraviolet bands become available, a quantitative analysis capable of distinguishing between cooling and stripping modes of star formation may be possible.

B.R.M would like to thank Mangala Sharma for helpful discussions. B.R.M. was supported by NASA Long Term Space Astrophysics Grant NAG5-11025 and Chandra Archival Research Grant AR2-3007X. S.S.M. was supported by NASA grant NAS8-01130. We thank the referee, Dr. Alastair Edge, for carefully reading the manuscript and offering suggestions that improved the presentation of the paper.

REFERENCES

- Allen, S. W. 2000, MNRAS, 315, 269
- Allen, S. W., Edge, A. C., Fabian, A. C., Böhringer, H., Crawford, C. S., Ebeling, H., Johnstone, R. M., Naylor, T., and Schwarz, R. A. 1992, MNRAS, 259, 67
- Basson, J. F., & Alexander, P. 2002, MNRAS submitted, astro-ph/0207668
- Böhringer, H., Matsushita, K., Churazov, E., Ikebe, Y., Chen, Y. 2002, AA, 382, 804
- Böhringer, H., Voges, W., Fabian, A. C., Edge, A. C., & Neumann, D. M. 1993, MNRAS, 264, L25
- Brüggen, M. 2003, astro-ph/0301352
- Brüggen, M., Kaiser, C. R., Churazov, E., & Enßlin, T. A. 2001, MNRAS, 2002, MNRAS, 331, 545
- Brüggen, M., Kaiser, C. R. 2002, Nature, 418, 301
- Brighenti, F. & Mathews, W. G. 2002, ApJ, 574, L11
- Burns, J. O. 1990, AJ, 99, 14
- Cardiel, N., Gorgas, J., & Aragon-Salamanca, A. 1998, MNRAS, 298, 977
- Carilli, C. L., Perler, R. A., & Harris, D. E. 1994, MNRAS, 270, 173
- Churazov, E., Brüggen, M., Kaiser, C. R., Böhringer, H., & Forman, W. 2001, ApJ, 554, 261
- Churazov, E., Sunyaev, R., Forman, W., & Böhringer, H. 2002, MNRAS, 332, 729
- Cowie, L.L., Hu, E. M., Jenkins, E. B., & York, D. G. 1983, ApJ, 272, 29
- Crawford, C. S., & Fabian, A. C. 1993, MNRAS, 265, 431
- Crawford, C. S., Allen, S. W., Ebeling, H., Edge, A. C., Fabian, A. C. 1999, MNRAS, 306, 857
- David, L. P., Nulsen, P. E. J., McNamara, B. R., Forman, W., Jones, C., Ponman, T., Robertson, B., Wise, M. 2001, ApJ, 557, 546
- De Young, D.S. 2003, MNRAS, 343, 719

- Donahue, M., Mack, J., Voit, G. M., Sparks, W. B., Elston, R., & Maloney, P. R. 2000, *ApJ*, 545, 670
- Edge, A. C. 2001, *MNRAS*, 328,762
- Edge, A. C., Wilman, R. J., Johnstone, R. M., Crawford, C. S., Fabian, A. C., & Allen, S. W. 2002, *MNRAS*, 337, 49
- Edge, A. C., Ivison, R. J., Smail, I., Blain, A. W., & Kneib, J. P. 1999, *MNRAS*, 306, 599
- Fabian, A. C. 1994, *ARAA*, 32, 277
- Fabian, A. C., Mushotzky, R. F., Nulsen, P. E. J., Peterson, J. R. 2000, *MNRAS*, 321, L20
- Fabian, A. C., Allen, S. W., Crawford, C. S., Johnstone, R. M., Morris, R. G., Sanders, J. S., & Schmidt, R. W. 2002, *MNRAS*, 332, L50
- Fabian, A. C., Voigt, L. M. & Morris, R. G. 2002, *MNRAS*, 335, L71
- Falcke, H., Rieke, M. J., Rieke, G. H., Simpson, C., Wilson, A. 1998, *ApJ*, 494, 155
- Gubanov, A. G. & Reshernikov, V. P., 1999, *AstL*, 25, 380
- Heckman, T. M., Baum, S. A., van Breugel, W. J. M., & McCarthy, P. J. 1989, *ApJ*, 338, 48
- Heinz, S., Reynolds, C. S., & Begelman, M. C. 1998, *ApJ*, 501, 126
- Jaffe, W. & Bremer, M. N. 1997, *MNRAS*, 284, L1
- Jaffe, W. & Bremer, M. N., & van der Werf, P. P. 2001, *MNRAS*, 324, 443
- Kaiser, C. R. & Binney, J. 2003, *MNRAS*, 338, 837
- Kennicutt, R. C., Jr. 1998, *ApJ*, 498, 541
- Mackie, G. 1992, *ApJ*, 400, 65
- Colafrancesco, S., Mewe, R., Forman, W. R. 2002, *ApJ*, 567, L37
- McNamara, B. R. 2002, in “The High Energy Universe at Sharp The High Energy Universe at Sharp Focus: Chandra Science,” San Francisco: ASP Conf. Ser., 262, 351, eds. S. Vrtilik, E. M. Schlegel, & L. Kuhi, astro-ph/0202199
- McNamara, B. R. 1997, in “Galactic and Cluster Cooling Flows,” San Francisco: ASP Conf. Ser., 115, 109, ed. N. Soker

- McNamara, B. R. & O’Connell, R. W. 1989, *AJ*, 98, 2018
- McNamara, B. R. & O’Connell, R. W. 1992, *ApJ*, 393, 579
- McNamara, B. R., Wise, M., Sarazin, C. L., Jannuzi, B. T., & Elston, R. 1996, *ApJ*, 466, L9
- McNamara, B. R., Wise, M., Nulsen, P. E. J., David, L. P., Sarazin, C. L., Bautz, M., Markevitch, M., Vikhlinin, A., Forman, W. R., Jones, C., & Harris, D. E. 2000, *ApJ*, 534, L135
- McNamara, B. R., Wise, M. W., Nulsen, P. E. J., David, L. P., Carilli, C. L., Sarazin, C. L., O’Dea, C. P., Houck, J., Donahue, M., Baum, S., Voit, M., O’Connell, R. W., Koekemoer, A. 2001, *ApJ*, 562, L149
- Molendi, S. & Pizzolato, F. 2001, *ApJ*, 560, 194
- Narayan, R. & Medvedev, M.V. 2001, *ApJ*, 562, 129
- Nulsen, P. E. J., David, L. P., McNamara, B. R., Jones, C., Forman, W.R., & Wise, M. 2002, *ApJ*, 568, 163
- O’Dea, C. P., Baum, S. A., & Gallimore, J. F. 1994, *ApJ*, 436, 669
- Peletier, R. F., Davies, R. L., Illingworth, G. D., Davis, L. E., & Cawson, M. 1990, *AJ*, 100, 1091
- Peterson, J. R., Paerels, F. B. S., Kaastra, J. S., Arnaud, M., Reiprich, T. H., Fabian, A. C., Mushotzky, R. F., Jernigan, J. G., Sakelliou, I. 2001, *A&A*, 365, L324
- Peterson, J. R., Kahn, S. M., Paerels, F. B. S., Kaastra, J. S., T. Tamura, J. A. M., Bleeker, & C. Ferrigno 2003, *ApJ*, submitted, astro-ph/0210662
- Porter, A. C., Schneider, D. P., Hoessel, J. G. 1991, *AJ*, 101, 1561
- Quilis, V., Bower, R. G., & Balogh, M. L. 2001, *MNRAS*, 328, 1091
- Reynolds, C. S., Heinz, S., & Begelman, M. C. 2002, *MNRAS*, 332, 271
- Rosner, R. & Tucker, W. H. 1989, *ApJ*, 338, 761
- Ruszkowski, M. & Begelman, M. C. 2002, *ApJ*, 573, 485
- Sanders, D. B., & Mirabel, I. F. 1996, *ARAA*, 34, 749

- Schombert, J. M. 1986, *ApJS*, 60, 603
- Silk, J., Djorgovski, S., Wyse, R. F. G., & Bruzual, G. A. 1986, *ApJ*, 307, 415
- Soker, N., White, R. E., III, David, L. P., & McNamara, B. R. 2001, *ApJ*, 549, 832
- Soker, N., Blanton, E. L., & Sarazin, C. L. 2003, in preparation
- Stevens, I. R., Acreman, D. M., & Ponman, T. J. 1999, *MNRAS*, 310, 663
- Taylor, G. B. 1996, *ApJ*, 470, 394
- Tucker, W., & David, L. P. 1997, *ApJ*, 484, 602
- Voigt, L. M., Schmidt, R. W., Fabian, A. C., Allen, S. W., & Johnstone, R. M., 2002, *MNRAS*, 335, L7
- Voit, G. M., & Donahue, M. 1997, *ApJ*, 486, 242
- White, R. L., Becker, R. H., Helfand, D. J., & Gregg, M. D. 1997, *ApJ*, 475, 479
- Wise, M. W., O’Connell, R. W., Bregman, J. N., & Roberts, M. S. 1993, *ApJ*, 405, 94
- Zakamska, N. L., & Narayan, R. 2003, *ApJ*, 582, 162

Table 1: Abell 1068 Photometry

| Feature | $m(R_g)$ | μ_g | $(U - R)_{K,0}$ | $\Delta\alpha$ | $\Delta\delta$ | Area(arcsec ²) |
|---------|----------|---------|-----------------|----------------|----------------|----------------------------|
| A | 15.89 | 20.63 | 1.81 | 0 | 0 | 78.7 |
| B | 17.83 | 21.67 | 2.07 | -3.3 | 6.1 | 34.4 |
| C | 18.03 | 22.49 | 1.62 | -11.8 | 1.4 | 60.8 |
| D | 16.94 | 21.02 | 2.32 | -12.7 | -7.1 | 42.9 |
| E | 18.53 | 21.02 | 2.29 | -23.0 | 20.7 | 9.91 |
| F | 21.89 | 22.63 | 1.90 | -20.2 | 16.5 | 1.98 |
| F | 22.55 | 23.30 | 1.82 | -16.9 | 13.2 | 1.98 |
| F | 22.30 | 23.05 | 1.88 | -13.6 | 9.9 | 1.98 |

Table 2: Star Formation Rates & Luminosity Masses

| History | $(U - R)_{AP}$ (mag) | $L(U)_{AP}$ (10 ¹⁰ L _⊙) | t (Myr) | M_{AP} (10 ⁸ M _⊙) | SFR (M _⊙ yr ⁻¹) |
|-------------|-------------------------|---|--------------|---|---|
| Nucleus | | | | | |
| Const | -0.3 | 2 | 10 | 4 | 40 |
| Burst | -0.3 | ... | 6 | 4 | – |
| Const | -0.1 | ... | 100 | 16 | 16 |
| Burst | -0.1 | ... | 40 | 10 | – |
| Off Nucleus | | | | | |
| Const | -0.2 | 0.5 | 100 | 5 | 5 |
| Burst | -0.2 | ... | 7 | 0.9 | – |
| Const | 0.1 | ... | 500 | 15 | 3 |
| Burst | 0.1 | ... | 50 | 3 | – |

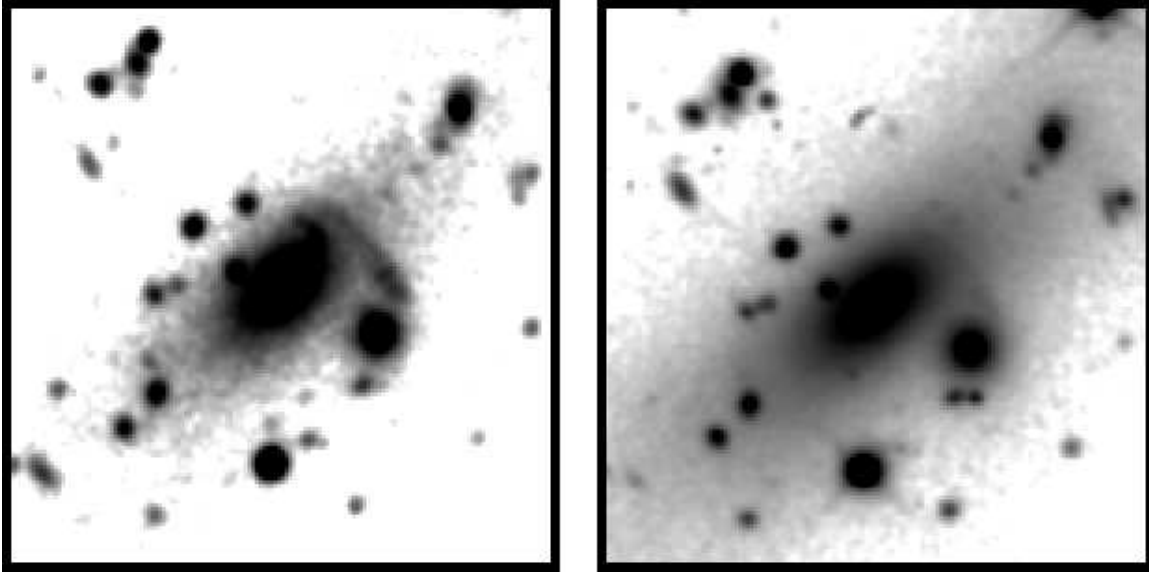


Figure 1: *U*-band image (left) and *R*-band image (right) of the central 1.2×1.2 arcmin of Abell 1068. North is toward the top; east is to the left.

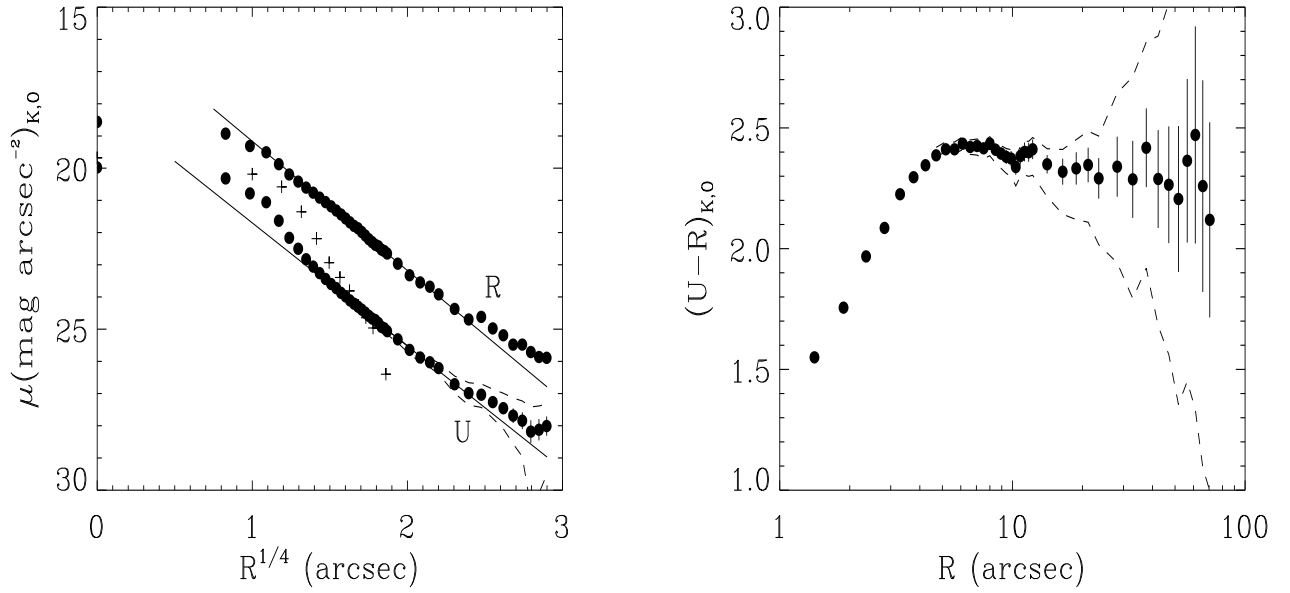


Figure 2: **left** U and R surface brightness profiles for the Abell 1068 cD. The solid lines represent $R^{1/4}$ -law profiles. The arbitrarily-scaled $H\alpha$ profile, is shown with “+” symbols. **right** $U - R$ color profile with systematic error envelope and statistical errors superposed.

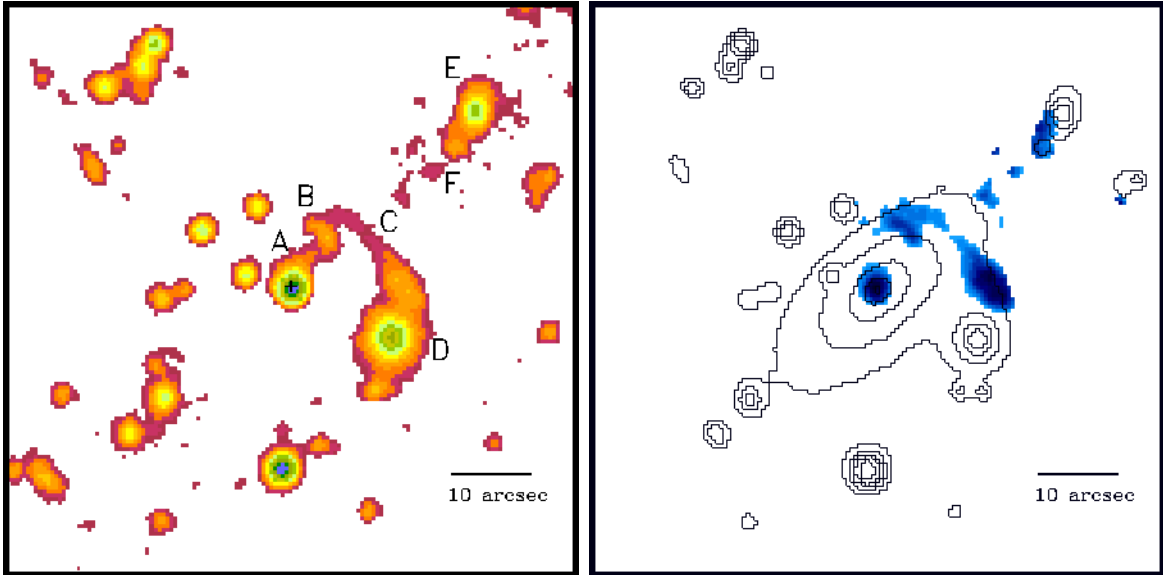


Figure 3: **left** The central 1.2×1.2 arcmin U -band image after subtracting the model central galaxy. The features discussed in the text are labeled. **right** $U - R$ color map with R -band contours superposed. The anomalously blue regions are shown in blue. North is toward the top; east is to the left.

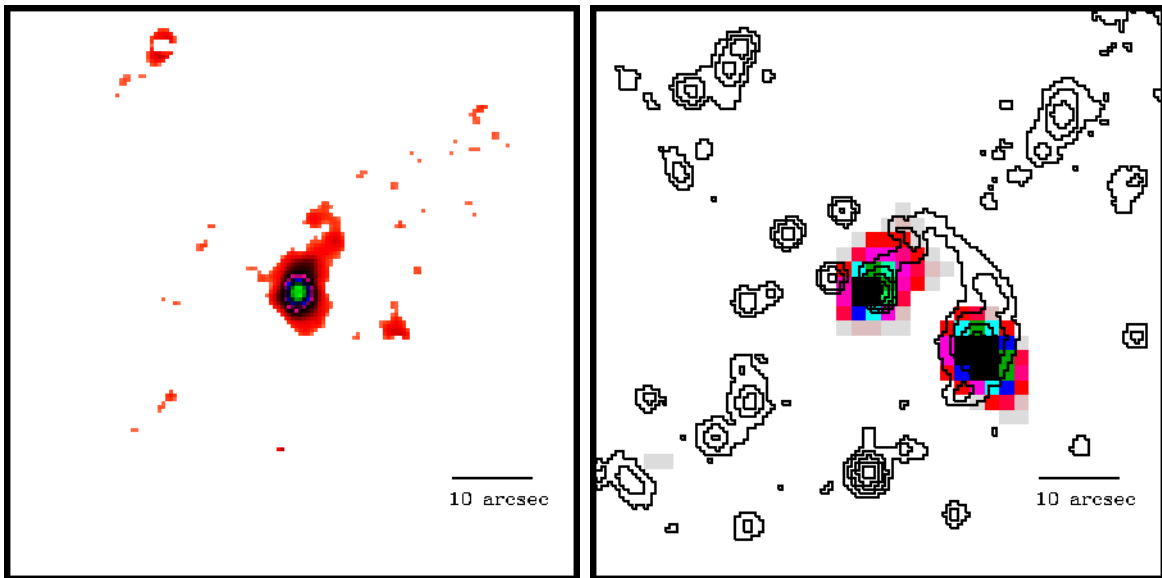


Figure 4: **left** The central 1.2×1.2 arcmin $H\alpha+N [II]$ map shown on the same scale as Fig. 3. **right** *FIRST* survey 20 cm radio image (color) superposed on *U*-band contours from Fig. 3. North is toward the top; east is to the left.

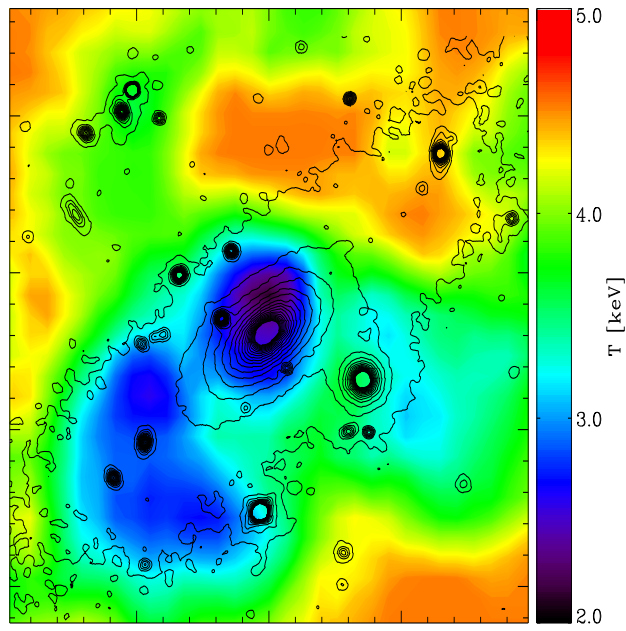


Figure 5: The central 1.2×1.2 arcmin temperature map constructed from the Chandra data described in WMM. The R -band contours showing the cD and neighboring galaxies is superposed. North is toward the top; east is to the left.

